Age of a prehistoric "Rodedian" cult site constrained by sediment and rock surface luminescence dating techniques

Sohbati, Reza; Murray, Andrew; Porat, N. ; Jain, Mayank; Avner, U.

Published in:
Quaternary Geochronology

Link to article, DOI:
10.1016/j.quageo.2015.09.002

Publication date:
2015

Document Version
Peer reviewed version

Accepted Manuscript

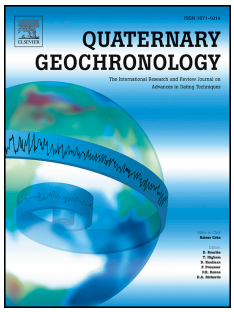

Age of a prehistoric “Rodedian” cult site constrained by sediment and rock surface luminescence dating techniques

R. Sohbati, A.S. Murray, N. Porat, M. Jain, U. Avner

PII: S1871-1014(15)30057-1

DOI: 10.1016/j.quageo.2015.09.002

Reference: QUAGEO 724

To appear in: *Quaternary Geochronology*

Received Date: 25 June 2015

Revised Date: 25 August 2015

Accepted Date: 3 September 2015

Please cite this article as: Sohbati, R., Murray, A.S., Porat, N., Jain, M., Avner, U., Age of a prehistoric “Rodedian” cult site constrained by sediment and rock surface luminescence dating techniques, *Quaternary Geochronology* (2015), doi: 10.1016/j.quageo.2015.09.002.

Age of a prehistoric "Rodedian" cult site constrained by sediment and rock surface luminescence dating techniques

R. Sohbati[a,b*], A.S. Murray[a], N. Porat[c], M. Jain[b], U. Avner[d]

[a]Nordic Laboratory for Luminescence Dating, Department of Geoscience, Aarhus University, DTU Risø Campus, Roskilde 4000, Denmark

[b]Center for Nuclear Technologies, Technical University of Denmark, DTU Risø Campus, Roskilde 4000, Denmark

[c]Geological Survey of Israel, 30 Malkhe Israel Street, Jerusalem 95501, Israel

[d]Dead Sea-Arava Science Center, Patio 655, Eilat 88133, Israel

[*]Corresponding author: resih@dtu.dk

Keywords: Quartz, Feldspar, OSL, IRSL, Rock surface dating, Luminescence-depth profile, Light attenuation

Abstract

The construction age of a pavement in a "Rodedian" prehistoric cult site in Negev desert, Israel, is established by determining the burial age of (i) a cobble used in the pavement, and (ii) the underlying sediment. The quartz OSL age and the K-feldspar corrected IR_{50} age from the sediment and the corrected IR_{50} and $pIRIR_{225}$ ages from the cobble surface are all consistent, and give an average age of 4.22±0.06 ka. Although the very similar ages indicate the reliability of the methods, these ages are ~3-4 ka younger than that expected for Rodedian sites. The IR_{50} and $pIRIR_{225}$ luminescence-depth profiles from the cobble indicate multiple exposure and burial events in the depositional history. The apparently young ages may thus represent a later intervention in the site during the late 3rd millennium B.C. More sites need to be dated by sampling of both rocks and sediments to confirm this suggestion. Important information on the bleaching history of the rock surfaces directly obtained from these luminescence-depth profiles is

not available in the underlying unconsolidated sediments. This is a significant advantage of rock surface dating over more conventional sediment dating.

1. Introduction

The settlement history of the Negev desert, Israel, has been traditionally described as a series of short periods of settlement interrupted by longer gaps. Archaeological sites were generally interpreted as temporary, seasonal and short-lived. However, with the advance of studies in the Negev, the settlement scenario is changing and gaps are shrinking (Avner, 2006). Of the Early Neolithic period (i.e. Pre-Pottery Neolithic periods B or PPNB, 8000-6400 BC) only about 30 habitation sites are currently known in the entire Negev (Barzilai & Goring-Morris, 2013) while almost no habitations are known from the Late Neolithic (LN, 6400-4600 BC). Nevertheless, during the last decade, 358 Neolithic cult sites were identified in the mountains of southern Negev, presently dated to the 7th and 6th millennia BC (Avner et al., 2014). These sites drastically change our view of human presence in the desert during the Early and Late Neolithic, as well as our understanding of their spiritual culture (Avner et al., 2014). The sites are named here "Rodedian" following the name of Naḥal Roded in the Eilat Mountains (~5 km NW of the Gulf of Aqaba), where the highest density of cult sites was found, up to 42 sites on an area of 0.8 km^2 (Fig. 1).

Establishing an absolute chronology for these sites has usually relied on the ^{14}C dating of associated organic remains; such material is not always available, and when it is, the association cannot always be assumed to be secure. Optically stimulated luminescence dating of rock surfaces has attracted significant interest in the last few years (Vafiadou et al., 2007; Sohbati et al., 2011; Simms et al., 2011; Liritzis et al., 2013; Sohbati, 2015). The great advantage of this technique over the more conventional luminescence dating of buried sediments is that rock surfaces usually record their depositional history. Habermann et al. (2000), Polikreti et al. (2002), Liritzis et al. (2010) and Sohbati et al. (2011, 2012a) have all measured luminescence signal with depth into rock surfaces that were exposed to light immediately before measurement. However, by measuring such luminescence profiles into a buried rock surface, one can determine the degree to which the surface had been bleached prior to burial (Sohbati et al., 2011, 2012a,b; Chapot et al., 2012) and even estimate, by using an appropriate calibration, how long the surface had been exposed before burial (Sohbati et al., 2012a; Freiesleben et al., 2015).

In this study we report the dating of a cult site at Naḥal Roded, using optically stimulated luminescence (OSL) of quartz, and infrared stimulated luminescence (IRSL) of potassium-rich feldspar fractions from the dust accumulated in the sediment trapped underneath a stone pavement. We support

the chronology of the sediment sample by IRSL dating of whole-rock slices from the buried surface of the rock.

2. The site and sampling

The site is located on a low Precambrian igneous ridge, formed by a quartz-porphyry dike. It contains several stone features, including a pavement, on which an anthropomorphic limestone image was found lying horizontally (Fig. 2). Flint flakes collected in the site suggest Late Neolithic date (i.e. 6th millennium BC). A small paving cobble (15×10×8 cm^3) and the dust accumulated underneath were collected under cover and placed in opaque plastic bags to prevent sample exposure to light. The light-protected sediment sample was accompanied by ~150 g of corresponding material for water content and dose rate measurements. The sediment sample is mixed with granite gruss; it is thus presumed that larger grain sizes are the product of local weathering and so not suitable for OSL dating, because of the expected low sensitivity and poor bleaching conditions.

3. Sample preparation and measurement facilities

The sediment sample was wet sieved into the size fraction 63-90 µm; this fraction is probably dominated by aeolian material, and presumed most likely to have been sufficiently bleached when deposited. The grains were treated with 10% HCl to remove carbonates and 10% H_2O_2 to dissolve any reactive organic material. They were then etched with 10% HF for 40 min to remove the alpha irradiated surface layer and weathering products and coatings, followed by 10% HCl for 20 min to remove any fluoride which may have precipitated. The K-rich feldspar fraction was then separated by floating in heavy liquid (ρ=2.58 $g.cm^{-3}$). Quartz grains (ρ>2.58 $g.cm^{-3}$) were further cleaned and etched using 40% HF for 1 h, followed by 10% HCl for 40 min. The resulting fractions were resieved (dry) into the grain size range mentioned above. From the cobble sample, cores of ~10 mm diameter and various lengths (>20 mm) were drilled using a water-cooled diamond-tipped core drill. These cores were then cut into slices of ~1.5 mm thick by a water-cooled low- speed wafering saw equipped with a 0.3 mm thick diamond blade. The surface slices (<1.5 mm depth) were treated similarly to the K-rich feldspar grains (using 10% HF for 40 min. and 10% HCl for 20 min) to ensure the removal of any surface weathering products. No acid treatment was done on inner slices.

All luminescence measurements were carried out using Risø OSL/TL reader (Model TL-DA 15). The blue (470 nm, 80 mW.cm^{-2}) stimulated signal from quartz grains was detected through a Hoya U-340 glass filter and the infrared (875 nm, 135 mW.cm^{-2}) stimulated signal from K-rich feldspar grains and intact cobble slices was measured through a Schott BG39/Corning 7-59 filter combination (2 and 4 mm, respectively). Beta irradiations used a ^{90}Sr/^{90}Y source mounted on the reader and calibrated for both disks and cups using 180-250 mm calibration quartz grains (Bøtter-Jensen et al., 2010; Hansen et al., 2015). To calibrate the source for rock slices, six slices cut from a quartzite cobble were sensitized and stabilized using successive cycles of dosing (~50 Gy) and heating (up to 450°C). They were then given an accurately known dose of 4.81 Gy using a ^{137}Cs gamma source in a scatter free geometry and measured using a single-aliquot regenerative (SAR) protocol (Murray and Wintle, 2000). Slices were directly placed on the disk positions in the carousel, whereas quartz grains were mounted as large (8 mm) and K-rich feldspar grains as small (2 mm) aliquots in a monolayer using silicone oil on stainless steel disks (quartz) and cups (feldspar). The heating rate was 5°C.s^{-1} throughout. All thermal treatments and stimulations at temperatures higher than 200°C were carried out in nitrogen atmosphere. The slices were held at the stimulation temperature for 30 s before the measurement started to allow the entire slice volume to reach the measurement temperature. This pause was 5 s for steel disks and cups. Five empty channels were inserted before and after the stimulation to monitor the isothermal thermoluminescence (TL).

4. Dosimetry

The radionuclide concentrations (^{238}U, ^{226}Ra, ^{232}Th and ^{40}K) in both the cobble and sediment samples were measured using high-resolution gamma spectrometry. The cobble and sediment sample (dried at 50°C) were first pulverized and homogenized. The sediment sample was heated to 450^{o}C for 24 h to remove any organic matter. The material was then cast in wax to prevent radon loss and to provide a reproducible counting geometry. Samples were stored for at least three weeks to allow ^{222}Rn to reach equilibrium with its parent ^{226}Ra before being measured on a high-purity Germanium detector for at least 24 h. Details of the gamma spectrometry calibration are given in Murray et al. (1987). The internal beta dose rate activity from ^{40}K in K-rich feldspar grains was calculated based on an assumed effective potassium content of 12.5±0.5% (Huntley & Baril, 1997), and the beta contribution from ^{87}Rb was calculated assuming a ^{87}Rb content of 400±100 ppm (Huntley & Hancock, 2001). A small internal alpha

contribution of 0.10±0.05 Gy.ka^{-1} from internal ^{238}U and ^{232}Th was also included in the dose rates, derived from ^{238}U and ^{232}Th concentration measurements by Mejdahl (1987). For quartz, an internal dose rate of 0.010±0.002 Gy.ka^{-1}was assumed (Vanderberghe et al., 2008). The radionuclide concentrations were converted to dose rate data using the conversion factors from Guérin et al. (2011). The contribution from cosmic radiation to the dose rate was calculated following Prescott and Hutton (1994), assuming an uncertainty of 5%. The long-term water content of the sediment sample was assumed to be 10% of the saturation water content. The saturated water content of the cobble is negligible. Water content, radionuclide concentrations and dry, infinite-matrix beta and gamma dose rates are summarized in Table 1.

4.1. Dose rate modeling modelling

In order to calculate the effective dose rate at the cobble/sediment interface, the variation of beta, gamma and so total dose rates with depth into both the cobble and sediment must be determined. Since the sampled cobble was part of a pavement, surrounded by other rocks of similar lithology, we model it as a homogeneous layer of thickness 8 cm (the actual thickness of the cobble) and effectively infinite extent. Beginning by assuming the sediment layer to be inert and the cobble layer as active, and following the expressions given by Aitken (1985: appendix H), the variation of beta dose rate in the sediment but arising from the cobble can be written as follows:

$$\dot{D}_{\beta,rock}^{sed} = 0.5\dot{D}_{\beta,rock}e^{-ax} \qquad (1)$$

where $\dot{D}_{\beta,rock}$ (Gy.ka^{-1}) is the beta infinite-matrix dose rate of the cobble, a (mm^{-1}) is the beta linear attenuation coefficient in sediment and x (mm) is the depth into sediment from the interface. Similarly, the variation of beta dose rate in the cobble due to its own internal radioactivity is given by:

$$\dot{D}_{\beta,rock}^{rock} = \dot{D}_{\beta,rock}\{1 - 0.5(e^{-bx} + e^{-b(h-x)})\} \qquad (2)$$

where b (mm^{-1}) is the beta linear attenuation coefficient in the cobble, and h (mm) is the thickness of the cobble layer. Similar expressions can be used to describe the gradient of the sediment beta dose rate in sediment and rock, and the gradient of the gamma dose rates into each medium arising from both rock and sediment, using the relevant infinite-matrix dose rates and linear attenuation coefficients. We calculated the beta linear attenuation coefficient in each medium, using a weighted average of the attenuation factors for uranium and thorium series reported by Aitken (1985; appendix H for a density of

2 g.cm^{-3}), and an assumed attenuation factor of 1.50 mm^{-1} for potassium. These attenuation factors were then modified by the assumed sediment and rock densities (2 and 2.6 g.cm^{-3}, respectively). The gamma linear attenuation coefficients were calculated by density modification of the coefficient obtained by fitting the variation of the weighted average of fractional doses of uranium, thorium and potassium with depth given by Aitken (1985: Table H.1). The calculated gamma and beta linear attenuation coefficients for each medium are given in Table 1. The overall variation of beta and gamma dose rates was then calculated using the principle of superposition (Aitken, 1985). Figure 3 shows the variation of beta, gamma and total dose rates through the sediment, cobble pavement and air. The total effective dose rate to surface slices from the cobble (depth <1.5 mm) and grains of sediment underlying the cobble (depth <10 mm), was calculated by integrating the total dose rate over the depth of interest.

There is no evidence that the cobble pavement has ever had a significant sediment cover. Nevertheless, had there been more than 30 cm of overlying sediment until just before sampling, the total dose rate at the rock/sediment interface of interest would have only increased by a maximum of 3%; this is considered negligible.

5. Results

5.1. Quartz

We applied a SAR protocol to measure the equivalent doses (D_e) using the OSL signal from the quartz fraction (Murray and Wintle, 2000). A preheat temperature of 260^{o}C for 10 s and a cut-heat (with immediate cooling) of 220^{o}C were used after the regeneration and test doses, respectively. All the OSL measurements were performed at 125^{o}C for 40 s. A further stimulation was carried out at 280^{o}C for 40 s at the end of each cycle to minimize the residual signal transfer between different cycles (Wintle and Murray, 2003). An outline of the OSL SAR protocol is given in Table 2. Signal intensities were calculated using the initial 0.8 s of the signal (channel=1-5), less a background derived from the following 1.6 s (channel=11-20). Data were collected in the 0.8 s preceding light stimulation (channel=1-5) to monitor any isothermal TL signal. An early background subtraction was chosen to minimize the contribution of the more difficult to bleach and more thermally unstable medium and slow components to the net signal (Jain et al., 2003; Li and Li, 2006; Pawley et al., 2010; Cunningham and Wallinga, 2010). We first examined the purity of our quartz extract by measuring the OSL signal from 6 aliquots with and without prior infrared stimulation at room temperature for 100 s and then calculated the

ratio of the two OSL signals, the so-called infrared (IR) depletion ratio (Duller et al., 2003). The resulting average IR depletion ratio was 0.95±0.01 (n=6), implying that any feldspar contamination in our sample is negligible.

For the dose recovery test, six aliquots were stimulated twice at room temperature for 100 s using blue LEDs, with a pause of 1 ks between the two stimulations to allow for any charge trapped in shallow refuge traps (especially that associated with the 110^{o}C TL peak) to decay and subsequently partly refill the OSL trap prior to the second stimulation; the aliquots were then given doses close to their equivalent doses (D_e). The measured-to-given dose ratio was 0.94±0.02 (n=6), showing that our protocol can accurately measure (i.e. within 10%) a known laboratory dose absorbed before any thermal pretreatment. The distribution of quartz OSL D_e values is shown in figure 4; the average equivalent dose is 20.2±1.0 Gy, which gives an age of 4.2±0.4 ka (Table 3).

5.2. K-rich feldspar

K-rich feldspar is an alternative dosimeter in luminescence dating; its use is increasing following the recent identification of more stable IRSL signals than used in earlier applications (Thomsen et al., 2008). These more stable post-IR IRSL (pIRIR) signals are measured after IR stimulation at close to ambient temperature (e.g. 50^{o}C). In addition, Murray et al. (2012) have argued that, by comparing quartz and K-feldspar equivalent doses, it is possible to identify those samples for which the quartz OSL was well-bleached at deposition. This argument is based on the widely-observed differential bleaching rates of quartz and feldspar signals (e.g. Godfrey-Smith et al., 1988; Thomsen et al., 2008; Buylaert et al., 2012; Murray et al., 2012; Sugisaki et al., 2015; Colarossi et al., 2015) when exposed to a daylight spectrum, and helps to quantitatively address one of the main uncertainties in the application of OSL to dating.

The D_e of K-rich feldspar was measured using a SAR protocol with a preheat of 260^{o} C for 60 s after both regenerative and test doses. The first IR stimulation at 50^{o}C (IR_{50}) was followed by a second IR stimulation at 225^{o}C ($pIRIR_{225}$) (Buylaert et al., 2009). The $pIRIR_{225}$ signal was chosen in preference to the more stable $pIRIR_{290}$ as it is easier to bleach (although still substantially more difficult than IR_{50} or quartz OSL). A high temperature stimulation at 280^{o}C was also performed at the end of each SAR cycle to minimize signal carry-over to the next SAR cycle. All IR stimulations were carried out for 200 s

(Buylaert et al., 2009; Sohbati et al., 2012c) (Table 2). The initial 1 s (channel=6-10) of stimulation less a background from the last 10 s (channel=946-995) was used for all calculations.

For dose recovery tests six aliquots were bleached using a Hönle SOL2 solar simulator for 4 h at a distance of ~80 cm (to avoid heating the samples). Three of these aliquots were then given a dose similar to the average $pIRIR_{225}$ D_e value of that sample (obtained from a test run) and measured. The remaining three aliquots were also measured (without adding a dose) to determine the amount of residual dose in the samples after bleaching in the laboratory. The IR_{50} and $pIRIR_{225}$ residual doses were 0.295±0.003 and 2.57±0.02 Gy (n=3), respectively. The ratio of the measured dose (after subtraction of the residual dose) to the given dose for the IR_{50} and $pIRIR_{225}$ signals was 1.00±0.02 (n=3) and 0.969±0.015 (n=3), respectively, showing that our feldspar protocol can also accurately measure (i.e. within 10%) a known laboratory dose absorbed before any thermal pretreatment. The average D_e values measured using IR_{50} and $pIRIR_{225}$ signals are 16.2±0.3 and 27.4±0.7 Gy, respectively (Fig. 5).

The athermal loss of IRSL signals in feldspars, the so-called anomalous fading, is usually quantified by the 'g'-value, which is the fractional loss of signal during a storage period of one decade of time, where the storage periods are expressed as decades relative to the laboratory irradiation time (Aitken 1985: appendix F). Here, fading rates were measured using SAR cycles (Table 2) on the same aliquots as used for D_e determination, following the approach of Auclair et al. (2003). A regenerative dose close to the $pIRIR_{225}$ D_e value and a test dose of ~0.5 D_e were used throughout. The ratios of regenerated signals (L_x) to test dose signals (T_x) were measured repeatedly, with the shortest possible time delays (i.e. prompt measurements) of ~0.18 h (IR_{50}) and ~0.26 h ($pIRIR_{225}$), and 12 h for delayed measurements. The 'g'-values were calculated using equation 4 of Huntley and Lamothe (2001) and normalized to a measurement delay time (t_c) of 2 days after irradiation. The average g_{2days} values for the IR_{50} and $pIRIR_{225}$ signals were 3.6±0.3 and 1.4±0.1 %/decade (n=3), respectively (Table 3). This observation is in agreement with earlier findings that the pIRIR signals are more stable than the IR signal measured at 50°C (Thomsen et al., 2008). The corrected IR_{50} age is 4.3±0.3 ka which is consistent with the quartz OSL age of 4.2±0.4 ka, while the corrected $pIRIR_{225}$ age of 5.9±0.4 ka is apparently older (Table 4). The older $pIRIR_{225}$ age is likely due to the fact that this signal bleaches more slowly than the quartz OSL and IR_{50} signal and thus may not have been well bleached at the time of deposition.

5.3. Rock slices

The buried bottom surface of the cobble used in the pavement must have been concealed from light at the same time as the corresponding underlying sediment, and thus should have a burial age similar to the sediment. In order to provide an additional constraint on the age of the pavement, we also measured the dose recorded by the buried surface of the cobble.

In the absence of a practical approach to separating quartz and K-feldspar grains without losing grain-size information, we chose to work with the IR signals from solid slices taken from the surface <1.5 mm layer. Several studies have shown that the infrared stimulated blue signal from feldspars mainly originates from K-rich grains (e.g. Baril and Huntley, 2003; Tsukamoto et al., 2012; Sohbati et al., 2013), and so the same protocol used for K-rich feldspar grains was applied to solid slices (see Table 2). The shape of the IRSL signals from the slices was similar to those of K-rich feldspar grains.

To examine the applicability of our measurement protocol to whole rock slices, a dose recovery test was carried out using six surface slices (<1.5 mm) from the top surface of the cobble, exposed to daylight at the time of sampling. Three of these slices were measured to give the average residual doses of 0.3±0.2 and 0.7±0.3 Gy (n=3) for the IR_{50} and $pIRIR_{225}$ signals, respectively. The other three slices were given a dose of ~20 Gy before measurement. The average IR_{50} and $pIRIR_{225}$ measured doses were 20.0±0.1 Gy and 19.0±0.1 Gy (n=3), giving a ratio of measured doses (less residual doses) to given dose of 0.99±0.01 and 0.92±0.01 (n=3), for the IR_{50} and $pIRIR_{225}$ signals, respectively. These ratios are within 10% of unity, suggesting that our protocol for the measurement of rock slices is appropriate.

The average IR_{50} and $pIRIR_{225}$ D_e values are 15.0±0.8 Gy and 24.8±0.6 Gy (n=8), respectively (Fig. 6). Anomalous fading was measured in a similar way to K-feldspar grains. The average g_{2days} values for the IR_{50} and $pIRIR_{225}$ signals were 7.5±0.4 and 2.1±0.2 %/decade (n=8), respectively (Table 3).

In order to provide the best estimate of the size of the luminescent K-feldspar grains in rock slices for dose rate calculation, a microscope viewfinder was calibrated using the large holes (500 µm) in a single grain disc. The diameter of 40 apparently K-rich feldspar grains was then measured. 75% of these grains (mostly perthite) had an average grain size of 610±140 µm, while the remaining 25% were larger crystals with an average size of 1200±300 µm resulting in an overall average grain size of ~770 µm. This is an order of magnitude larger than the average grain size of ~77 µm (63-90 µm) for K-feldspar grains from the sediment sample. Assuming a ^{40}K concentration of 12.5±0.5% (Huntley & Baril, 1997) and a

^{87}Rb content of 400±100 ppm (Huntley & Hancock, 2001), the internal beta dose rate in rock and sedimentary grains is ~2.8 and ~0.3 Gy.ka^{-1}, respectively.

The IR_{50} and $pIRIR_{225}$ fading corrected ages from the surface slices are 4.3±0.3 ka and 4.1±0.2, respectively (Table 3). These ages are indistinguishable from the quartz OSL and K-feldspar IR_{50} ages from the underlying sediment (Table 3). Considering the notable difference between the bleaching rates of these signals, the great consistency between the ages implies that the IR_{50} and $pIRIR_{225}$ signals in the cobble surface must have been as well reset as the OSL and IR_{50} signals in the underlying sediment, while the $pIRIR_{225}$ signal from the sediment may suffer from incomplete bleaching.

6. Was the cobble surface bleached?

In order to check whether the luminescence signal at the surface of the cobble was fully zeroed before it was incorporated into the pavement, we examined the variation of the natural sensitivity-corrected IR_{50} and $pIRIR_{225}$ signals (L_n/T_n s) with depth into the buried side of the cobble by measuring slices (1.5 mm thick) from three cores (of different lengths) drilled into the cobble (Fig. 7). Unfortunately, due to the shape and fragility of the cobble, we were unable to drill cores deeper than 25 mm into this sample, and the longest core broke during slicing, so that slices between 17 and 22 mm were lost. Nevertheless, the available data are very informative. Both IR_{50} and $pIRIR_{225}$ profiles show a gentle rise, followed by flattening and subsequently a steep rise towards signal saturation with depth. However, the normalized $pIRIR_{225}$ natural signals (L_n/T_n) increase towards saturation closer to the surface than do the IR_{50} signals (Fig. 7). This is consistent with earlier reports that elevated temperature pIRIR signals are more difficult to bleach than the IR_{50} signal (e.g. Sohbati et al., 2012c; Buylaert et al., 2012; Kars et al., 2014). On closer inspection, one can see a step in the luminescence profiles of both signals; at about ~4-5 mm for the $pIRIR_{225}$ signals and ~4-10 mm for the IR_{50}. Such steps are probably indicators of multiple burial and exposure events in the exposure history of the cobble (Freiesleben et al., 2015). The complex nature of the profiles and the variation of total dose rate with depth into the cobble (see Fig.3), necessitates modelling for an analytical description.

Freiesleben et al. (2015) have further developed the model of Sohbati et al. (2012d) to include multiple sequential exposure and burial events in a unified equation in which the parameters have physical meaning (in contrast to simple mathematical parametrization, e.g. Laskaris and Liritzis, 2011). Following their approach of assuming that charge trapping during exposure periods is negligible and the

dose rate during discrete burial events does not change, we use the equation below to fit our data (see Fig. 8).

$$L(x) = \left(\overbrace{\left(\overbrace{e^{-t_{e1}\overline{\sigma\varphi_0}e^{-\mu x}}}^{1st\ exposure\ event} - 1 \right) e^{-\frac{\dot{D}(x)}{D_o}t_{b1}} + 1}^{1st\ burial\ event} \right) e^{-t_{e2}\overline{\sigma\varphi_0}e^{-\mu x}} - 1 \Bigg) e^{-\frac{\dot{D}(x)}{D_o}t_{b2}} + 1 \quad (3)$$

This equation accounts for four sequential events; two exposure events (i.e. t_{e1} and t_{e2}) each followed by a burial event (i.e. t_{b1} and t_{b2}), t_{b2} is the time elapsed since final emplacement of the cobble in the pavement. $\overline{\sigma\varphi_0}$ is the rate of decrease of luminescence at the surface of the cobble (ka^{-1}) as a result of daylight exposure (see Sohbati et al., 2011), μ is the light attenuation factor (mm^{-1}), and $\dot{D}(x)$ is the dose rate (Gy.ka^{-1}) which is assumed to be the same during both burial events. The parameters values derived from the best fit of Eqn. 3 to the data are given in Table 4.

In order to estimate the degree of bleaching of the cobble surface before the final emplacement in the pavement, one can use the fitted values to predict the shapes of the profiles resulting from the last exposure event (t_{e2}) immediately before burial. The predicted profiles show that the IR_{50} and $pIRIR_{225}$ signals were almost certainly completely reset to depths of ~7 and ~2 mm, respectively, before the cobble was incorporated in the pavement (Fig. 8). Thus we can be confident that the D_e values measured from the surface slices do not include any poorly-bleached material (no significant residual doses) and, from that point of view at least, should be reliable.

7. Discussion

Considering the significant difference between the bleaching rates of quartz OSL and K-feldspar IR_{50} and $pIRIR_{225}$ signals, the remarkable agreement between the corrected IR_{50} and $pIRIR_{225}$ ages from the cobble surface and the OSL and corrected IR_{50} ages from the underlying sediment indicates that all these signals must have been well bleached before the cobble was emplaced in the pavement (Table 3). The older $pIRIR_{225}$ age from the sediment probably indicates that this signal was not as well reset as the corresponding signal from the cobble surface, perhaps, in part, because of the sampling depth of the sediment sample. The sediment underlying the cobble was an inhomogeneous mixture of fine grain

aeolian dust and coarse grain gruss produced by *in-situ* weathering of granitic cobbles. Thus, in order to obtain enough material in the fine grain range, the sediment was coarsely sampled up to a depth of ~1 cm using a flat trowel. It is certainly possible that the more difficult-to-bleach $pIRIR_{225}$ signal was not completely reset in the grains coming from several mm below the surface. This is in contrast to the cobble surface where complete bleaching of both IR_{50} and $pIRIR_{225}$ signals is not only supported by the agreement between the ages obtained from the two signals, but also by an independent modelling of their luminescence-depth profiles (Fig. 8).

From the luminescence-depth profile model, the length of the burial and exposure events (t_bs and t_es) could be derived, at least in principle, from the fitting of equation 3 to the data. This would require a knowledge of the value of parameters D_o and $\overline{\sigma\varphi_0}$ in the terms t_b/D_o and $\overline{\sigma\varphi_0}t_e$ (see Equation 3 and Table 4). The average IR_{50} and $pIRIR_{225}$ D_o values from the dose response curves of the surface slices are 200±20 and 149±14 Gy (n=8), respectively. Using these values and the values obtained from the fitting for t_{b1}/D_o (Table 4), give the IR_{50} and $pIRIR_{225}$ burial ages of 3.7±0.5 and 5.0±0.3 ka for event t_{b1}. These ages are of the same order of the last burial event (i.e. t_{b2}) of ~4.2 ka derived from the surface of the cobble and the underlying sediment. The IR_{50} and $pIRIR_{225}$ ages for the last burial event (i.e. t_{b2}) can be calculated in a similar way. The calculated $pIRIR_{225}$ age is 4.2±0.2 ka which is in excellent agreement with the ages obtained directly from the surface slices and the underlying sediment, while the IR_{50} age of 6.7±0.1 is somewhat older. The differences presumably arise because the assumption that a single D_o value applies to all aliquots is not strictly true; we take the burial age of ~4.2 ka derived from surface slices as the most reliable because the dose response curves were measured individually for these aliquots.

One could also obtain an exposure age from the luminescence depth profile if the decay rate at the surface ($\overline{\sigma\varphi_0}$) were known. One practical way to obtain an estimate of $\overline{\sigma\varphi_0}$ is to use a sample of known exposure age for calibration (Sohbati et al., 2012b; Freiesleben et al., 2015). Although we did not have access to such a sample, the technique can still be used to estimate the relative length of the two exposure events. The presence of a step in our profiles means that the first exposure event (t_{e1}) must have been longer than the second one (t_{e2}), as it has reset the signal to a deeper depth (Fig. 8). In general, such step profiles are only produced if the later exposure event is of shorter or similar length to the previous

event(s). Otherwise, the more recent event would completely overwrite the previous profile and thus delete all information on prior events.

8. Conclusions

We have established the construction age of a pavement in a "Rodedian" prehistoric cult site by determining the burial age of (i) a cobble used in the pavement and (ii) the underlying sediment. Quartz OSL age and K-feldspar IR_{50} corrected age from the sediment and the IR_{50} and $pIRIR_{225}$ corrected ages from the cobble surface all converge toward an age of ~4.2 ka. This is in agreement with the age of other stone structures such as prehistoric animal traps known as 'desert kites' and carnivore traps in the area (Holzer et al., 2010, Porat et al., 2013).

The very similar ages obtained from both the cobble surface and the underlying sediment indicates the reliability of the method. However, these ages are ~3-4 ka younger than that expected for the "Rodedian" sites. Although *ad-hoc* flint tools found in the sites can be dated to the 6^{th}-3^{rd} millennium BC (Late Neolithic through Early Bronze IV), none of the 357 sites presently surveyed yielded any pottery sherd dated to the time suggested by the luminescence ages. This is the first attempt to date a "Rodedian" site by means of OSL, and it is possible that these apparently young OSL ages represent a later intervention in the site during the late 3rd millennium B.C. This suggestion is consistent with the exposure and reburial events identified in the luminescence profile from the cobble. More sites need to be dated by sampling of both rocks and sediments to confirm this suggestion.

This study adds to the increasing evidence that OSL dating of rock surfaces is a robust and reliable dating technique. The invaluable information on the bleaching history of the rock surfaces that is directly obtained from luminescence-depth profiles is not available in unconsolidated sediments. This is a significant advantage of rock surface dating over more conventional sediment dating.

Acknowledgments

RS thanks Carlsberg Foundation for financial support (Grant no. 2012_01 _0838) during this project.

References

Aitken, M. J. (1985). Thermoluminescence Dating. 359 pp. *Academic Press*, London.

Auclair, M., Lamothe, M. & Huot, S. (2003). Measurement of anomalous fading for feldspar IRSL using SAR. *Radiation Measurements 37*, 487–492.

Avner U 2006. Settlement patterns in theWadi Arabah and the adjacent desert areas: a view from the Eilat region. In *Crossing the rift: resources, routes, settlement patterns and interaction in the Wadi Arabah*, Bienkowski P, Galor K (eds). Oxbow Books: Oxford; Levant Supplementary Series vol. 3: 51-74.

Avner, U., Shem-Tov, M., Enmar, L., Ragolski, G., Shem-Tov, R., Barzilai, O. (2014). A survey of Neolithic cult sites in the Eilat mountains, Israel. *Journal of the Israel Prehistoric Society*, *44*, 101–106.

Baril, M.R., & Huntley, D.J. (2003). Infrared stimulated luminescence and phosphorescence spectra of irradiated feldspars. Journal of Physics: *Condensed Matter 15*, 8029-8048.

Barzilai, O., & Goring-Morris, A. N. (2013). An estimator for bidirectional (naviform) blade productivity in the Near Eastern Pre-Pottery Neolithic B. *Journal of Archaeological Science*, *40*(1), 140–147. doi:10.1016/j.jas.2012.06.025

Buylaert, J. -P., Murray, A. S., Thomsen, K. J., & Jain, M. (2009). Testing the potential of an elevated temperature IRSL signal from K-feldspar. *Radiation Measurements*, *44*(5-6), 560–565. doi:10.1016/j.radmeas.2009.02.007

Buylaert, J.-P., Jain, M., Murray, A. S., Thomsen, K. J., Thiel, C., & Sohbati, R. (2012). A robust feldspar luminescence dating method for Middle and Late Pleistocene sediments. *Boreas*, *41*, 435–451. doi:10.1111/j.1502-3885.2012.00248.x

Bøtter-Jensen, L., Thomsen, K. J., & Jain, M. (2010). Review of optically stimulated luminescence (OSL) instrumental developments for retrospective dosimetry. Radiation Measurements, 45(3-6), 253–257. doi:10.1016/j.radmeas.2009.11.030

Chapot, M. S., Sohbati, R., Murray, A. S., Pederson, J. L., & Rittenour, T. M. (2012). Constraining the age of cobble art by dating a cobblefall event using sediment and cobble-surface luminescence dating techniques. *Quaternary Geochronology*, *13*, 18–25. doi:10.1016/j.quageo.2012.08.005

Colarossi, D., Duller, G. a. T., Roberts, H. M., Tooth, S., & Lyons, R. (2015). Comparison of paired quartz OSL and feldspar post-IR IRSL dose distributions in poorly bleached fluvial sediments from South Africa. *Quaternary Geochronology*, 1–6. doi:10.1016/j.quageo.2015.02.015

Cunningham, A. C., & Wallinga, J. (2010). Selection of integration time intervals for quartz OSL decay curves. *Quaternary Geochronology*, *5*(6), 657–666. doi:10.1016/j.quageo.2010.08.004

Duller, G. A. T. (2003). Distinguishing quartz and feldspar in single grain luminescence measurements. *Radiation Measurements*, *37*(2), 161–165. doi:10.1016/S1350-4487(02)00170-1

Godfrey-Smith, D., Huntley, D., & Chen, W. (1988). Optical dating studies of quartz and feldspar sediment extracts. *Quaternary Science Reviews*, *7*, 373–380.

Guérin, G., Mercier, N., & Adamiec, G. (2011). Dose-rate conversion factors : update. *Ancient TL*, *29*(1), 5–8.

Habermann, J., Schilles, T., Kalchgruber, R., & Wagner, G. A. (2000). Steps towards surface dating using luminescence. *Radiation Measurements*, *32*(5-6), 847–851. doi:10.1016/S1350-4487(00)00066-4

Hansen, V., Murray, A., Buylaert, J.-P., Yeo, E.-Y., & Thomsen, K. (2015). A new irradiated quartz for beta source calibration. *Radiation Measurements*, 1–5. doi:10.1016/j.radmeas.2015.02.017

Holzer, A., Avner, U., Porat N**.** & Horwitz, L.K. (2010). Desert kites in the Negev desert and northeast Sinai: Their function, chronology and ecology. *Journal of Arid Environments, 74*, 806-817.

Huntley, D. J. & Baril, M. R. (1997). The K content of the K-feldspars being measured in optical dating or in thermoluminescence dating. *Ancient TL*, *15*, 11–13.

Huntley, D. J. & Hancock, R. G. V. (2001). The Rb contents of the K-feldspar grains being measured in optical dating. *Ancient TL, 19*, 43–46.

Huntley, D. J. & Lamothe, M. (2001). Ubiquity of anomalous fading in K-feldspars and the measurement and correction for it in optical dating. *Canadian Journal of Earth Sciences*, *38*, 1093–1106.

Jain, M., Murray, a. S., & Bøtter-Jensen, L. (2003). Characterisation of blue-light stimulated luminescence components in different quartz samples: implications for dose measurement. *Radiation Measurements*, *37*(4-5), 441–449. doi:10.1016/S1350-4487(03)00052-0

Kars, R. H., Reimann, T., Ankjaergaard, C., & Wallinga, J. (2014). Bleaching of the post-IR IRSL signal: new insights for feldspar luminescence dating. *Boreas*, *43*(4), 780–791. doi:10.1111/bor.12082

Li, B., & Li, S.-H. (2006). Comparison of estimates using the fast component and the medium component of quartz OSL. *Radiation Measurements*, *41*(2), 125–136. doi:10.1016/j.radmeas.2005.06.037

Laskaris, N., & Liritzis, I. (2011). A new mathematical approximation of sunlight attenuation in rocks for surface luminescence dating. *Journal of Luminescence*, *131*(9), 1874–1884. doi:10.1016/j.jlumin.2011.04.052

Liritzis, I., Polymeris, G., & Zacharias, N. (2010). Surface luminescence dating of "Dragon Houses" and Armena Gate at Styra (Euboea, Greece). *Mediterranean Archaeology & Archaeometry*, *10*(3).

Liritzis, I, Singhvi, A.K, Feathers, J.K, Wagner, G.A, Kadereit, A, Zacharias, N, and Li, S-H (2013) Luminescence Dating in Archaeology, Anthropology and Geoarchaeology: An Overview. SpringerBriefs in Earth System Sciences.

Mejdahl, V. (1987). Internal radioactivity in quartz and feldspar grains. *Ancient TL*.

Murray, A. S., Marten, R., Johnston, A. & Martin, P. (1987). Analysis for naturally occurring radionuclides at environmental concentrations by gamma spectrometry. *Journal of Radioanalytical and Nuclear Chemistry*, *115*, 263–288.

Murray, A. S., & Wintle, A. G. (2000). Luminescence dating of quartz using an improved single-aliquot regenerative-dose protocol. *Radiation Measurements*, *32*, 3–7.

Murray, A. S., & Wintle, A. G. (2003). The single aliquot regenerative dose protocol: potential for improvements in reliability. *Radiation Measurements*, *37*(4-5), 377–381. doi:10.1016/S1350-4487(03)00053-2

Murray, A. S., Thomsen, K. J., Masuda, N., Buylaert, J. P., & Jain, M. (2012). Identifying well-bleached quartz using the different bleaching rates of quartz and feldspar luminescence signals. *Radiation Measurements*, *47*(9), 688–695. doi:10.1016/j.radmeas.2012.05.006

Pawley, S. M., Toms, P., Armitage, S. J., & Rose, J. (2010). Quartz luminescence dating of Anglian Stage (MIS 12) fluvial sediments: Comparison of SAR age estimates to the terrace chronology of the Middle Thames valley, UK, *Quaternary Geochronology*, *5*, 569–582, doi:10.1016/j.quageo.2009.09.013.

Polikreti, K., & Michael, C. (2002). Authenticating marble sculpture with thermoluminescence. *Ancient TL, 20*(I), 11–18.

Porat, N., Avner, U., Holzer, A., Shemtov, R., & Horwitz, L.K. (2013). Fourth Millennium BC 'leopard traps' from the Negev Desert (Israel). *Antiquity* 87, 714-727.

Preusser, F., Ramseyer, K., & Schlüchter, C. (2006). Characterisation of low OSL intensity quartz from the New Zealand Alps. *Radiation Measurements, 41*(7-8), 871–877. doi:10.1016/j.radmeas.2006.04.019.

Prescott, J. R. & Hutton, J. T. (1994). Cosmic ray contributions to dose rates for luminescence and ESR dating: large depths and long-term variations. *Radiation Measurements, 23*, 497–500.

Sawakuchi, A. O., Blair, M. W., DeWitt, R., Faleiros, F. M., Hyppolito, T., & Guedes, C. C. F. (2011). Thermal history versus sedimentary history: OSL sensitivity of quartz grains extracted from cobbles and sediments. *Quaternary Geochronology, 6*(2), 261–272. doi:10.1016/j.quageo.2010.11.002

Simms, A. R., DeWitt, R., Kouremenos, P., & Drewry, A. M. (2011). A new approach to reconstructing sea levels in Antarctica using optically stimulated luminescence of cobble surfaces. *Quaternary Geochronology, 6*(1), 50–60. doi:10.1016/j.quageo.2010.06.004

Sohbati, R., Murray, A. S., Jain, M., Buylaert, J.-P., & Thomsen, K. J. (2011). Investigating the resetting of OSL signals in rock surfaces. *Geochronometria, 38*(3), 249–258. doi:10.2478/s13386-011-0029-2

Sohbati, R., Murray, A. S., Chapot, M.S., Jain, M., & Pederson, J. (2012a). Optically stimulated luminescence (OSL) as a chronometer for surface exposure dating. *Journal of Geophysical Research, 117*(B9), B09202. doi:10.1029/2012JB009383

Sohbati, R., Murray, A. S., Buylaert, J.-P., Almeida, N. A. C., & Cunha, P. P. (2012b). Optically stimulated luminescence (OSL) dating of quartzite cobbles from the Tapada do Montinho archaeological site (east-central Portugal). *Boreas, 41*, 452–462. doi:10.1111/j.1502-3885.2012.00249.x

Sohbati, R., Murray, A. S., Buylaert, J.-P., Ortuño, M., Cunha, P. P., & Masana, E. (2012c). Luminescence dating of Pleistocene alluvial sediments affected by the Alhama de Murcia fault (eastern Betics, Spain) - a comparison between OSL, IRSL and post-IR IRSL ages. *Boreas, 41*(2), 250–262. doi:10.1111/j.1502-3885.2011.00230.x

Sohbati, R., Jain, M., & Murray, A. (2012d). Surface exposure dating of non-terrestrial bodies using optically stimulated luminescence: A new method. *Icarus*, *221*, 160–166.

Sohbati, R., Murray, A., Jain, M., Thomsen, K., Hong, S.-C., Yi, K., & Choi, J.-H. (2013). Na-rich feldspar as a luminescence dosimeter in infrared stimulated luminescence (IRSL) dating. *Radiation Measurements*, *51-52*, 67–82. doi:10.1016/j.radmeas.2012.12.011

Sohbati, R. (2015). Luminescence, Rock Surfaces. *Encyclopedia of Scientific Dating Methods*. Springer Netherlands, 485-488. doi:10.1007/978-94-007-6326-5_83-4

Sugisaki, S., Buylaert, J.-P., Murray, A., Tada, R., Zheng Hongbo, Ke, W., … Irino, T. (2015). OSL dating of fine-grained quartz from Holocene Yangtze delta sediments. *Quaternary Geochronology*, 1–7. doi:10.1016/j.quageo.2015.02.021

Thomsen, K., Murray, A. S, Jain, M., & Bøtter-Jensen, L. (2008). Laboratory fading rates of various luminescence signals from feldspar-rich sediment extracts. *Radiation Measurements*, *43*(9-10), 1474–1486. doi:10.1016/j.radmeas.2008.06.002

Tsukamoto, S., Nagashima, K., Murray, a. S., & Tada, R. (2011). Variations in OSL components from quartz from Japan sea sediments and the possibility of reconstructing provenance. *Quaternary International*, *234*(1-2), 182–189. doi:10.1016/j.quaint.2010.09.003

Tsukamoto, S., Jain, M., Murray, A.S., Thiel, C., Schmidt, E., Wacha, L., & Frechen, M. (2012). A comparative study of the luminescence characteristics of polymineral fine grains and coarse grained K- and Na-rich feldspars. *Radiation Measurements*, *47*, 903-908.

Vafiadou, a, Murray, a, & Liritzis, I. (2007). Optically stimulated luminescence (OSL) dating investigations of rock and underlying soil from three case studies. *Journal of Archaeological Science*, *34*(10), 1659–1669. doi:10.1016/j.jas.2006.12.004

Vandenberghe, D., De Corte, F., Buylaert, J.-P., Kučerac, J. & Vanden Haute, P. (2008). On the internal radioactivity in quartz. *Radiation Measurements*, *43*, 771–775.

Figure captions

Figure 1: Location of cult sites distributed around Naḥal Roded in the Eilat Mountains, Israel

Figure 2: A view of the studied cobble pavement. The red arrow shows the collected sample.

Figure 3: The variation of (a) beta, (b) gamma and (c) total dose rates across the sediment, cobble and air. The blue and red lines in (a) and (b) show the dose rates due to the cobble and sediment, respectively. The blue, red and black lines in (c) represent gamma, beta and total dose rates, respectively. The dose rate in each medium due to itself is shown with a solid line and that in its adjacent media with a dashed line. The vertical dash lines represent the boundaries between the media.

Figure 4: The distribution of quartz OSL equivalent doses.

Figure 5: The distribution of K-rich feldspar IR_{50} and $pIRIR_{225}$ equivalent doses.

Figure 6: The distribution of IR_{50} and $pIRIR_{225}$ equivalent doses from the surface slices (<1.5 mm) from the buried bottom side of the cobble.

Figure 7: The variation of the natural sensitivity-corrected IR_{50} and $pIRIR_{225}$ signals with depth into the buried surface of the cobble. Each data point denotes the L_n/T_n value measured from a 1.5 mm thick slice coming from a certain depth into the cobble and thus represents the average luminescence at a particular depth. The data points up to a depth of 10 mm represent an average of three values measured from slices coming from three parallel cores. The missing data at depth 16-22 mm is because the longest core broke during slicing.

Figure 8: a) The same data as in Fig. 7 normalized to the corresponding saturation limit (the average of the deepest three points) for each signal. The solid lines show the fitting of the model (Eqn. 3) to the data and the dashed lines represent the 95% confidence bands. b) The IR_{50} predicted profiles (dashed lines) obtained by using the parameter values in Table 4 in the relevant part of Eqn. 3. The solid line shows the present day profile as fitted by the model. c) The same data as in (b) for the $pIRIR_{225}$ signal.

Table captions

Table 1: Summary of the radionuclide concentrations and beta and gamma attenuation factors used to calculate the effective dose rates. Feldspar dose rates assume a K concentration of 12.5±0.5% for K-feldspar grains (Huntley & Baril 1997). The water content in the sediment sample was assumed to be 10% of the saturated water content. Uncertainties represent one standard error.

Table 2: Outline of the quartz OSL (Murray and Wintle, 2003) and K-feldspar post-IR IRSL SAR protocols (Buylaert et al., 2009).

Table 3: Summary of D_e values, fading rates, effective dose rates and uncorrected and corrected ages for the cobble and the underlying sediment.

Table 4: The parameters used in the model and their obtained values from the fitting. Both data sets were fitted simultaneously using the global curve fitting function in OriginPro 9. The light attenuation factor μ was shared as a fixed, signal-independent parameter between the two fits. $\overline{\sigma\varphi_0}t_e$s and t_b/D_os were considered as single parameters in order to reduce the number of variables in the model.

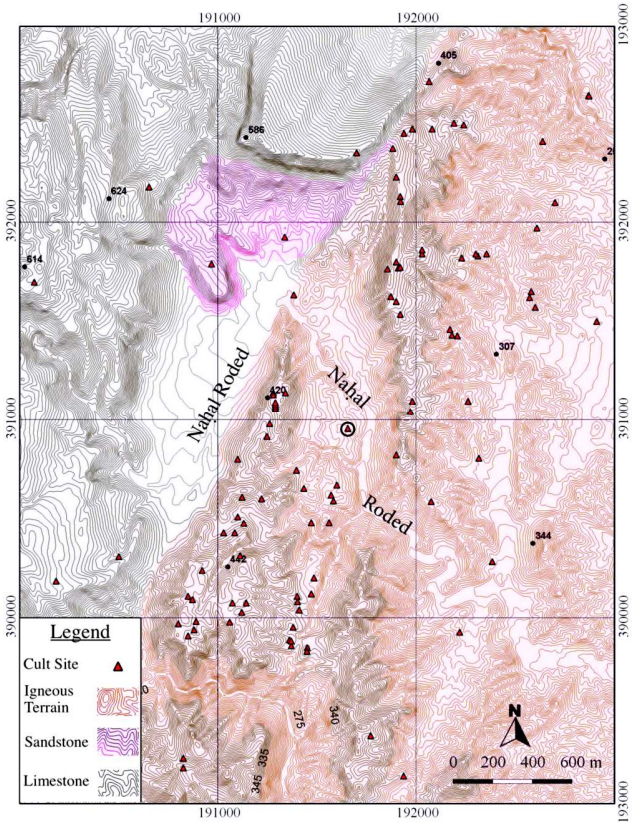

Figure 1

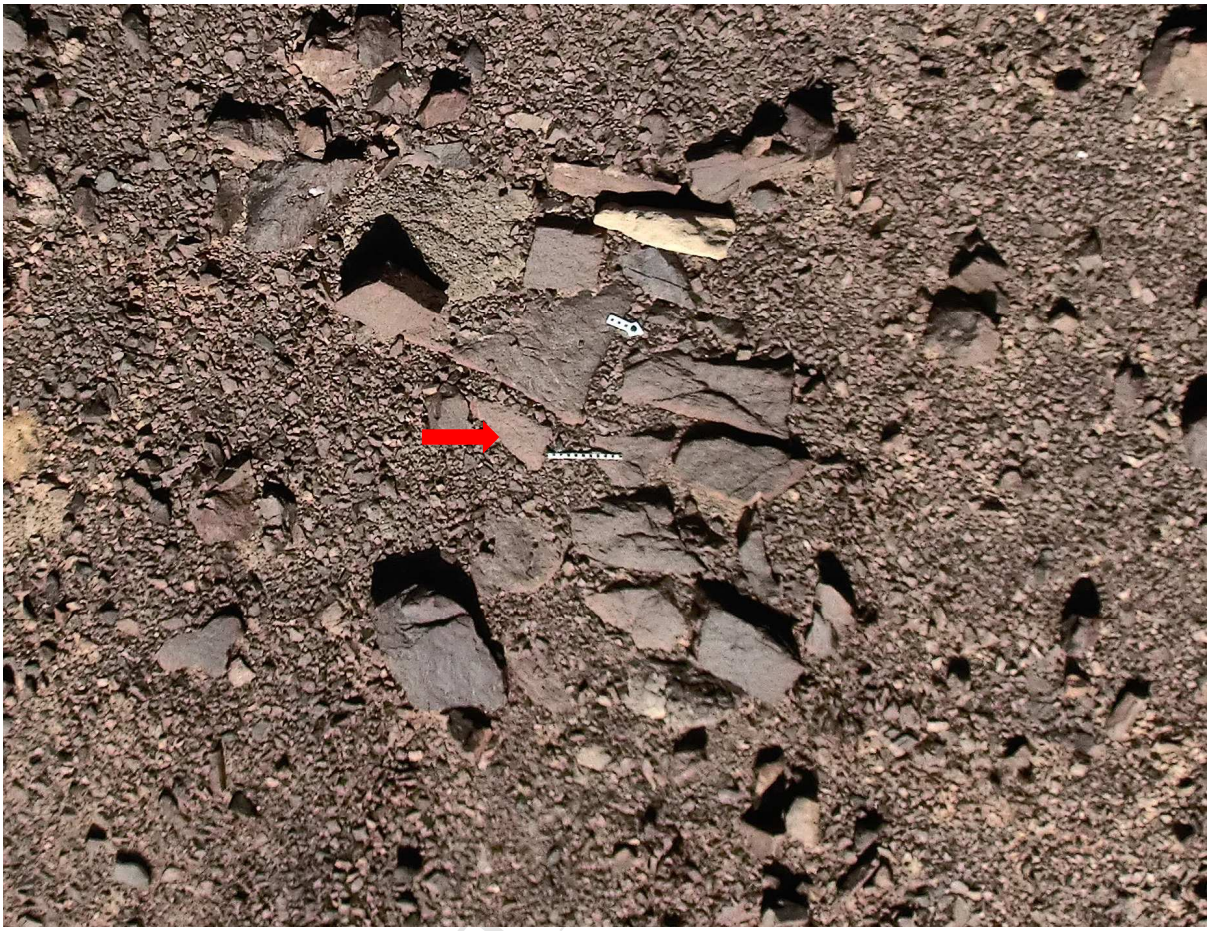

Figure 2

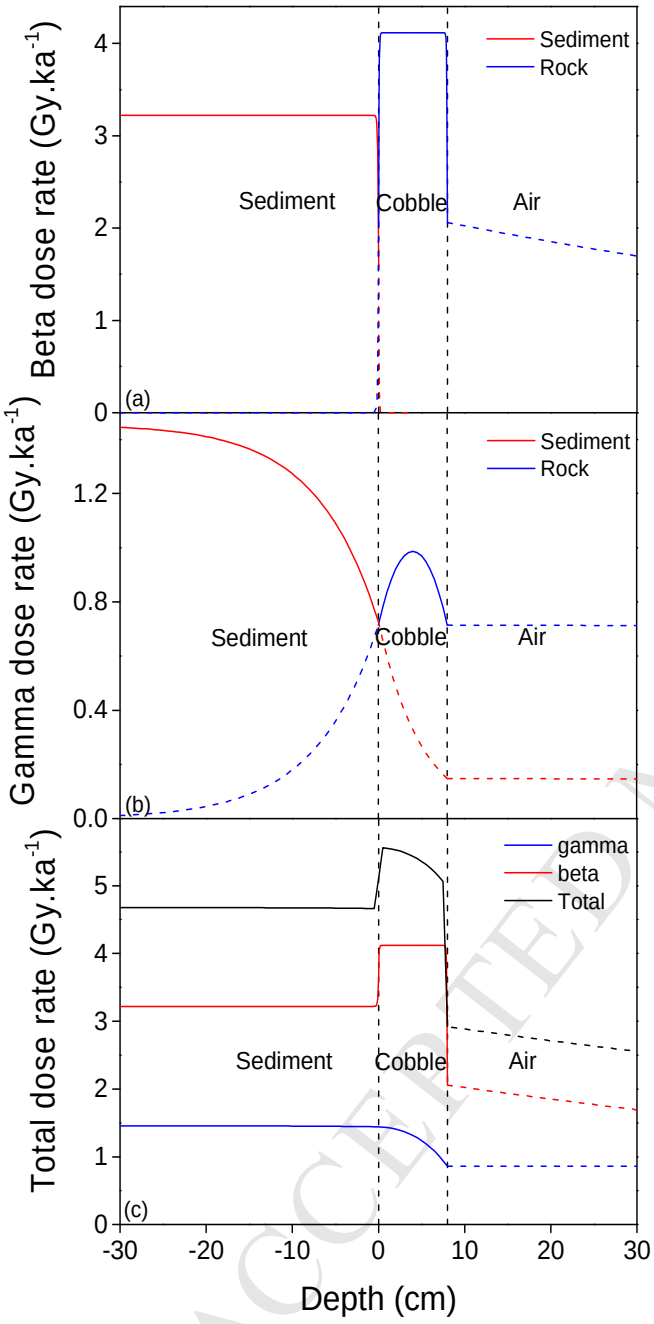

Figure 3

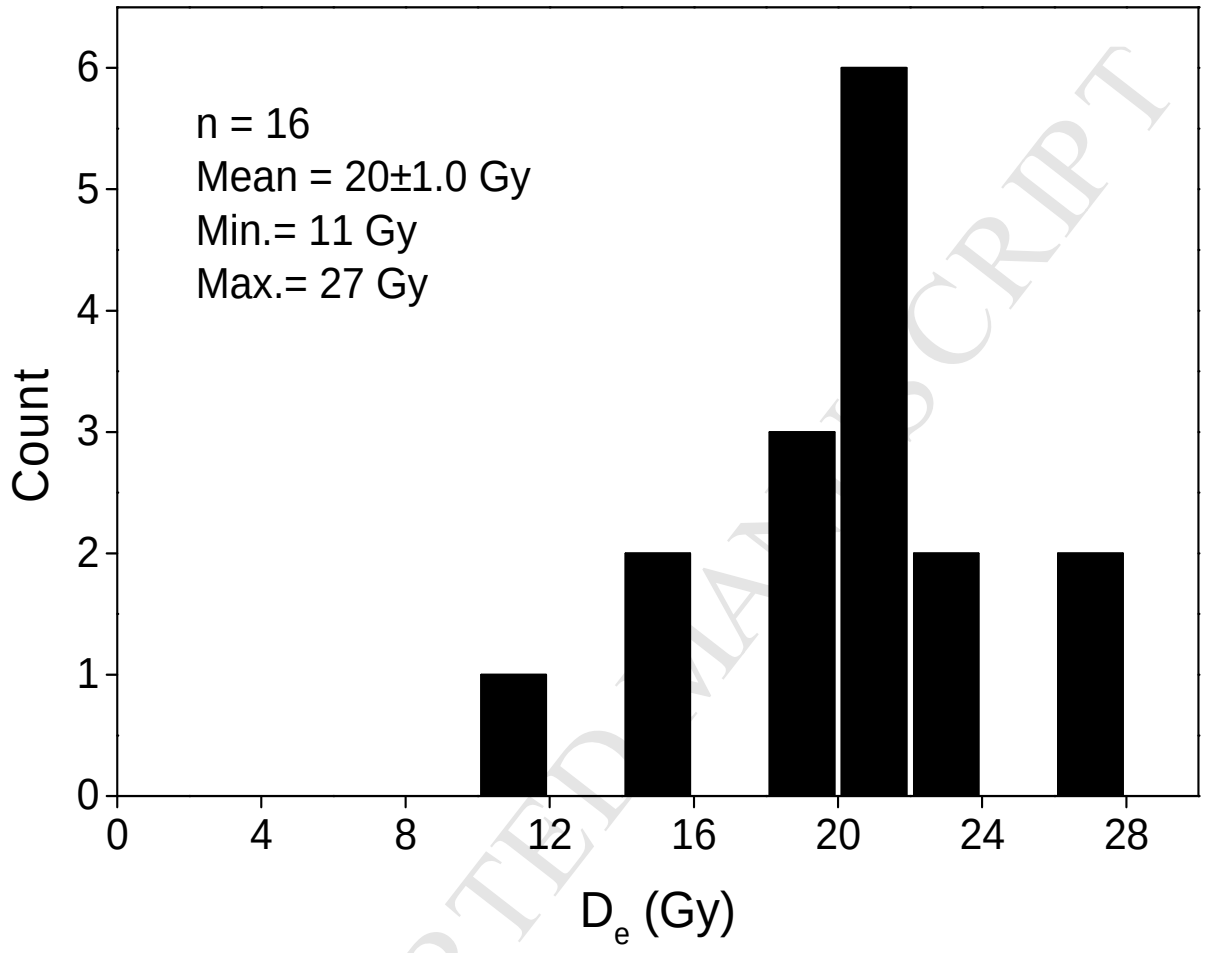

Figure 4

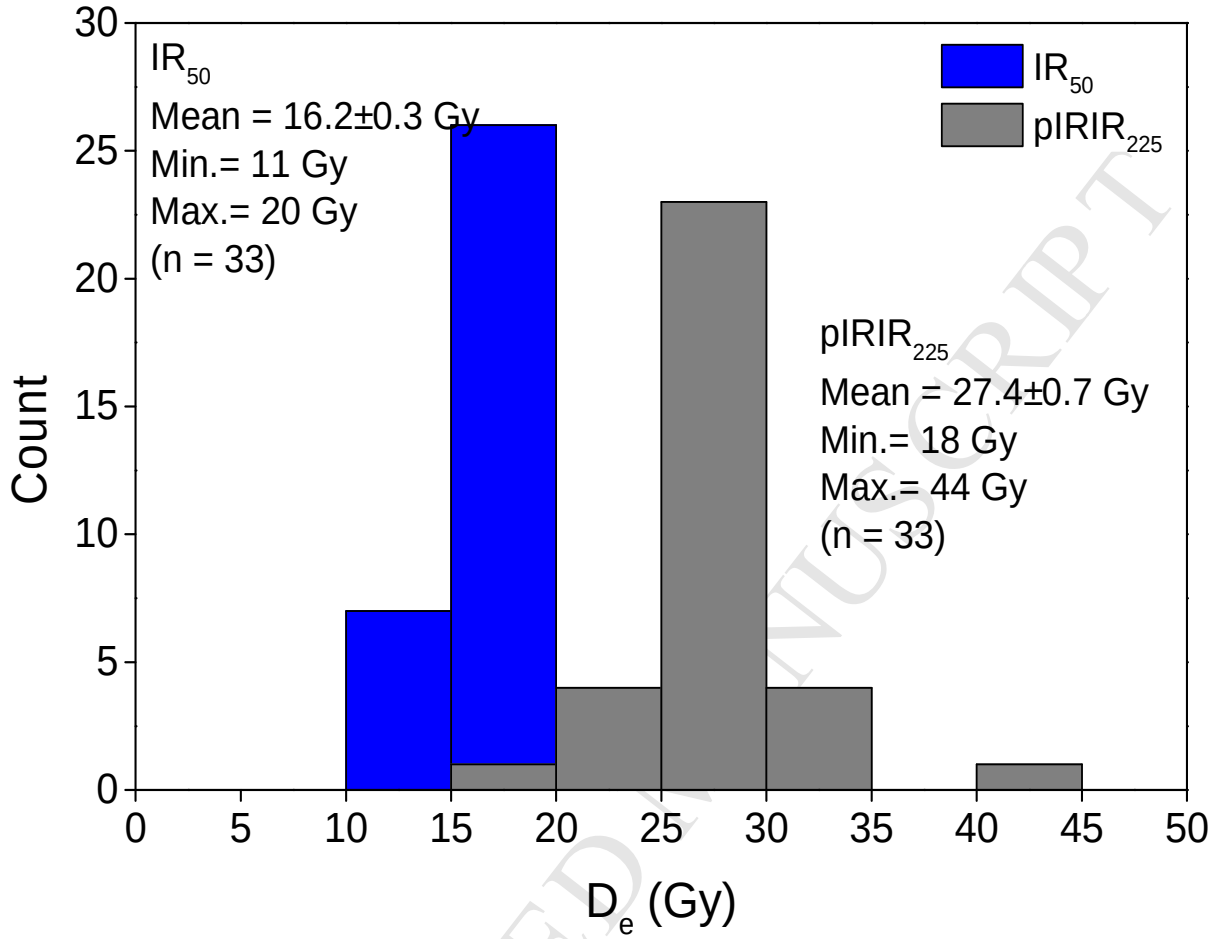

Figure 5

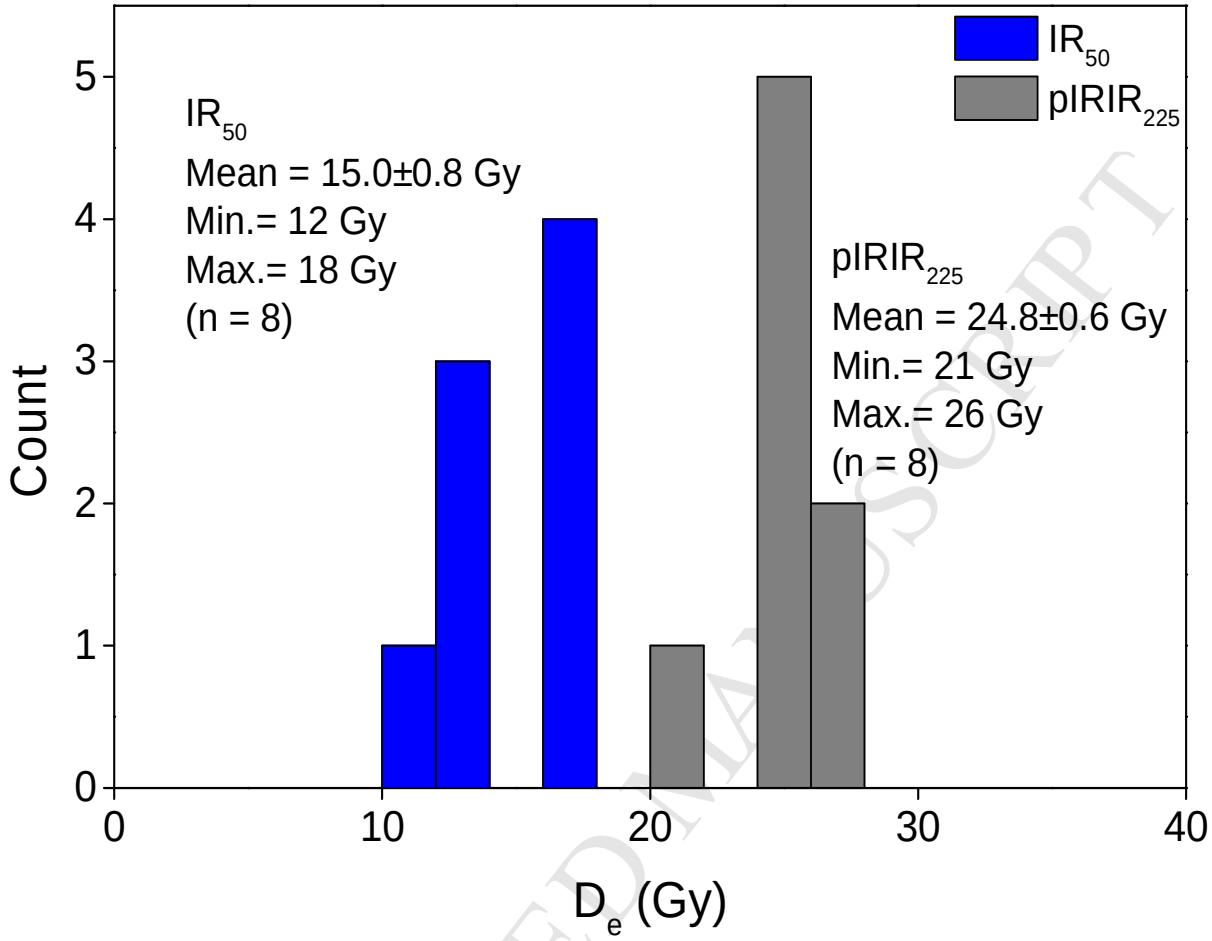

Figure 6

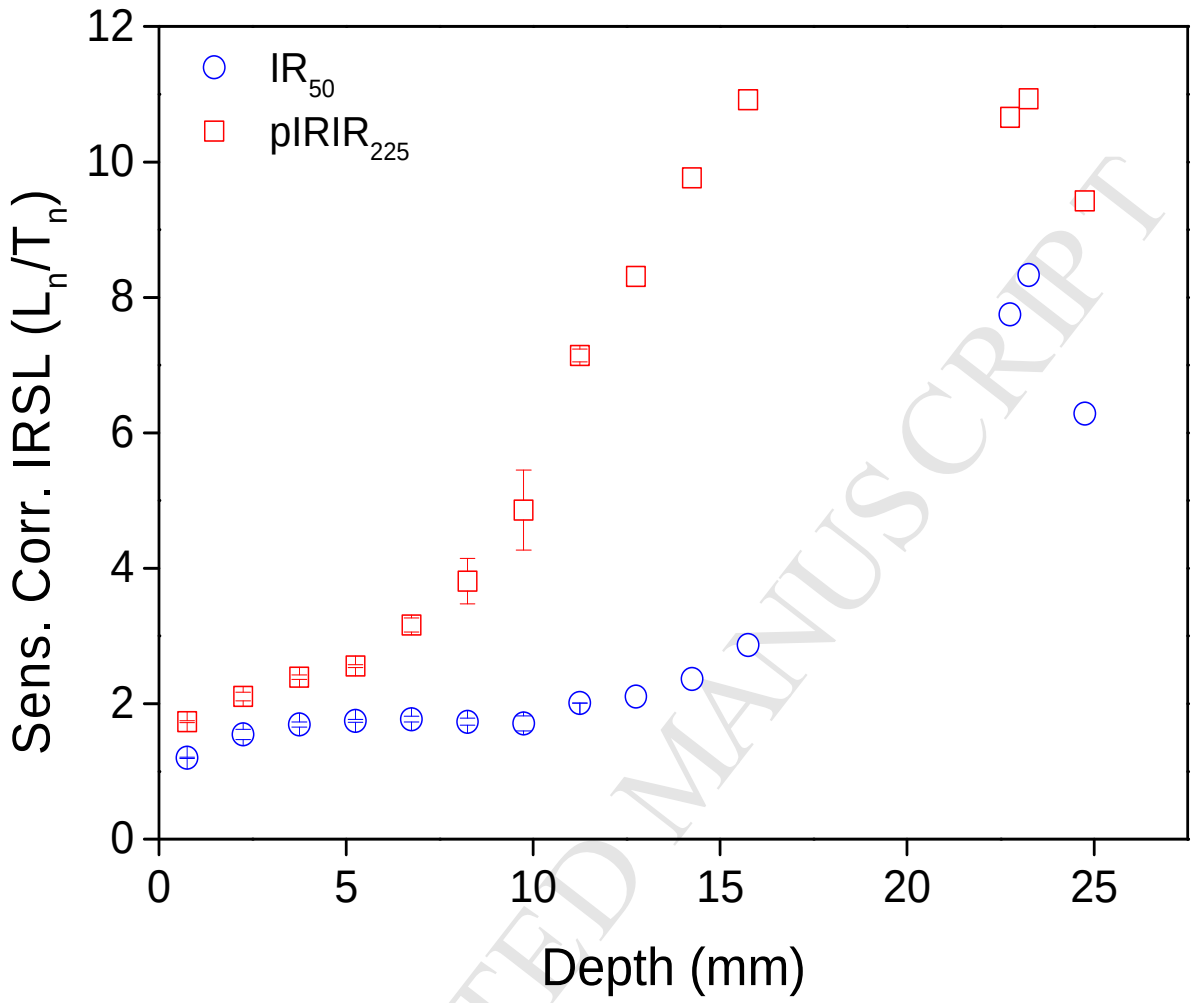

Figure 7

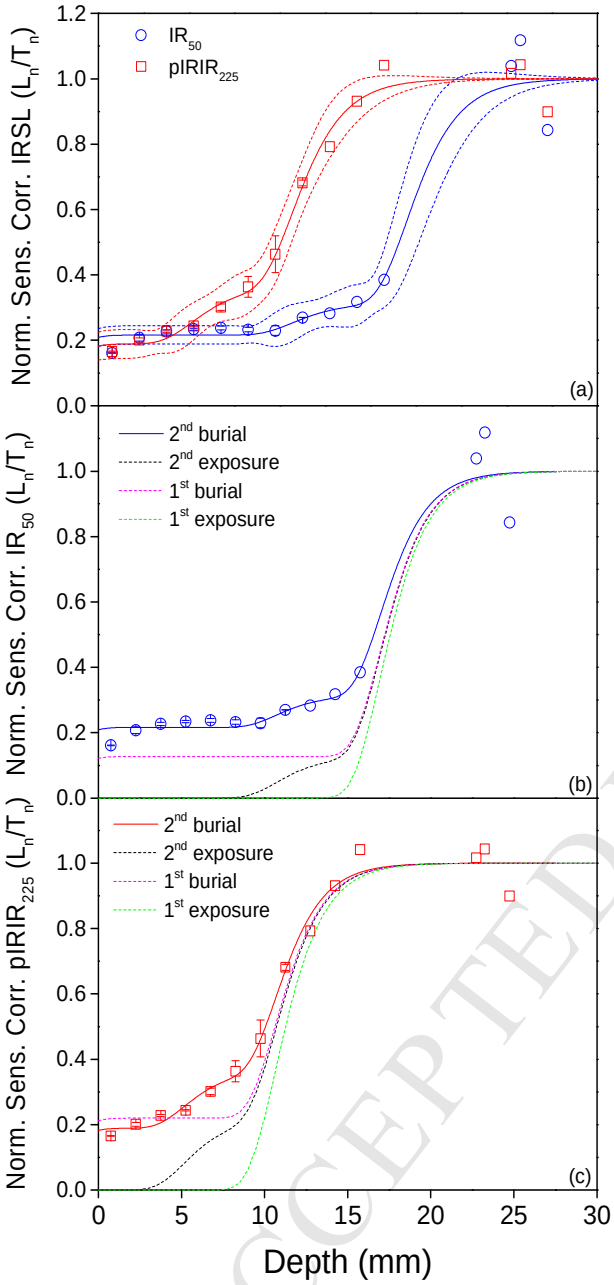

Figure 8

Sample	Water content	^{238}U	^{226}Ra	^{232}Th	^{40}K	Beta dose rate	Beta atten. factor	Gamma dose rate	Gamma atten. factor
	(%)	(Bq kg^{-1}) ± se	(Bq kg^{-1}) ± se	(Bq kg^{-1}) ± se	(Bq kg^{-1}) ± se	(Gy ka^{-1}) ± se	(mm^{-1})	(Gy ka^{-1}) ± se	(cm^{-1})
Sediment	1.5±1.5	21.8±10.8	29.5±0.9	34.6±1.1	1104±24	3.28±0.08	1.46	1.48±0.03	0.15
Cobble	0	30.2±7.5	21.8±0.6	44.9±0.8	1410±24	4.12±0.07	1.9	1.79±0.03	0.2

Table 1

Step	Quartz		K-feldspar & Slices	
	Treatment	Observed	Treatment	Observed
1	Dose		Dose	
2	Preheat (260^{o}C for 10 s)		Preheat (260^{o}C for 60 s)	
3	Blue stimulation (125^{o}C for 40 s)	L_x	Infrared stimulation (50^{o}C for 200 s)	$L_{x,\ IR50}$
4	-------		Infrared stimulation (225^{o}C for 200 s)	$L_{x,\ pIRIR225}$
5	Test dose		Test dose	
6	Cut heat (220^{o}C)		Preheat (260^{o}C for 60 s)	
7	Blue stimulation (125^{o}C for 40 s)	T_x	Infrared stimulation (50^{o}C for 200 s)	$T_{x,IR50}$
8	-------		Infrared stimulation (225^{o}C for 200 s)	$T_{x,\ pIRIR225}$
9	Blue stimulation (280^{o}C for 40 s)		Infrared stimulation (280^{o}C for 200 s)	
10	Return to 1		Return to 1	

Table 2

Sample	Quartz				Feldspar									
	D_e, OSL	Age	n	Dose rate	D_e, IR_{50}	Uncorrected IR_{50} age	Fading rate	Corrected IR_{50} age	D_e, $pIRIR_{225}$	Uncorrected $pIRIR_{225}$ age	Fading rate	Corrected $pIRIR_{225}$ age	n	Dose rate
	(Gy) ±se	(ka) ±se		($ka.Gy^{-1}$) ±se	(Gy) ±se	(ka) ±se	g_{2days} (%/dec.) ±se	(ka) ±se	(Gy) ±se	(ka) ±se	g_{2days} (%/dec.) ±se	(ka) ±se		($ka.Gy^{-1}$) ±se
Sediment	20.2±1.0	4.2±0.4	16	4.77±0.17	16.2±0.3	3.13±0.14	3.6±0.3	4.3±0.2	27.4±0.7	5.3±0.3	1.4±0.1	5.9±0.3	33	5.18±0.18
Cobble	----	----	----	----	15.0±0.8	2.1±0.1	7.2±0.2	4.3±0.4	24.8±0.6	3.4±0.3	2.1±0.2	4.1±0.2	8	7.24±0.2

Table 3

Parameter	IR_{50}	se	$pIRIR_{225}$	se	Units
t_{b1}/D_o	0.019	0.009	0.034	0.011	$ka.Gy^{-1}$
$\overline{\sigma\varphi_o}t_{e1}$	3.37×10^4	7.98×10^4	702	1155	---
μ	0.61	0.14	0.61	0.14	mm^{-1}
$\overline{\sigma\varphi_o}t_{e2}$	706	1274	24	25	---
t_{b2}/D_o	0.033	0.002	0.029	0.004	$ka.Gy^{-1}$

Table 4